Injection into a Circular Machine with a KV Distribution*

RECEIVED

FEB 0 8 1996

OSTI

E. Crosbie and K. Symon[1]

Argonne National Laboratory, 9700 South Cass Avenue, Argonne, IL 60439 USA

Abstract. In order to achieve a maximum space charge limit in the IPNS-II synchrotron it is desirable to inject a Kapchinskij-Vladimirskij (KV) distribution (1). We rederive the KV distribution, first starting from a smoothed Hamiltonian and then for the full alternating gradient case. The microcanonical distribution can be generalized slightly so as to allow one to alter the aspect ratio of the beam ellipse.

The KV distribution requires that the injected particles all have the same total transverse oscillation energy, and also that they are distributed uniformly throughout the entire energy shell. This requires painting the injected beam uniformly in the three independent dimensions of the energy shell. We have devised two scenarios for doing this, one involving a suitable variation of the x and y injected amplitudes during the injection process, and the second involving introducing a small coupling between the x and y motions.

We have written a program to simulate the injection process which includes the turn-to-turn forces between the (500) injected turns. If we omit the turn-to-turn forces then the resulting space charge density distributions are indeed very nearly uniform within a circular beam cross section for either KV injection scenario, but are neither uniform nor circular for other plausible scenarios. With turn-to-turn forces included, the interturn scattering can be fairly important and the resulting density distributions tend to develop lower density halos.

If we add a gradient bump to simulate magnetic quadrupole errors in the lattice, then the effects of half-integral resonances can be clearly seen. When the space charge forces between turns depress the tune to a resonance, beam growth keeps the tunes constant at the edge of the stop band, unless the resonance is crossed quickly. The resultant growth of the beam can be seen in the density distribution if resonant effects are dominant, i.e. starting with tunes near the resonance. If we start farther from the resonance, in which case we inject higher intensity beams, the turn-to-turn forces dominate the final density distribution. In that case the final distribution is nearly the same whether the resonance is present or not, though the effect of the resonance on the final tune can still be clearly seen.

MASTER

DISCLAIMER

Portions of this document may be illegible
in electronic image products.   Images are
produced from the best available original
document.

I. INTRODUCTION

The Kapchinskij-Vladimirskij (KV) distribution (1) was originally of mathematical interest as a many particle problem which could be solved analytically. It gave an idea of the effects of space charge forces in high intensity accelerators, but it was not expected that any real accelerator would contain a microcanonical distribution.

Recently it has been suggested that the KV distribution may be of practical interest for high intensity machines in that it may provide the maximum space charge limit for such a machine. One can make a plausible argument that the maximum beam intensity is obtained for a distribution for which all particles have the same tune, at least when the resonance is approached. One should therefore first reduce the chromaticity of the accelerator ring as much as possible, and second, make the betatron frequencies independent of amplitude, i.e., make the focussing forces linear. One way to make the focussing forces linear is to start with external focussing forces which are linear, and then make the space charge forces also linear by using a KV distribution.

Chapter II reviews the theory of the KV distribution, generalizing it slightly to include an elliptical beam cross section. We give first a simplified treatment based on treating the betatron oscillations as simple harmonic motions. We then treat the alternating gradient case. Finally two injection scenarios are described which produce a KV distribution (if beam-beam interactions are neglected during the injection process). In the first the injected x and y amplitudes follow a prescribed schedule. In the second there is a coupling between the x and y motions.

We have written a simulation code for the injection process which includes the space charge interactions between the injected turns. It also provides a gradient bump to simulate the effect of quadrupole errors which can drive a half-integral resonance. The code was used to study the injection process for the proposed IPNS upgrade (2), a 2 GeV rapidly cycling synchrotron designed to deliver a 1 MW proton beam. During the injection process 500 turns are injected. Chapter III presents the results of simulating the injection process, without turn-to-turn space charge forces, for a KV scenario and for a typical injection scenario which is not specifically designed to produce a KV distribution. The KV scenario indeed produces a circular beam cross section of uniform density. Non-KV scenarios produce a beam cross section which is neither circular nor of uniform density.

In describing the injection process we will use the following terminology. We will specify a time by the number of turns (revolutions of the beam around the accelerator) since injection started. The beam at any time consists of a number of beamlets. By a beamlet we mean that part of the beam which was injected during a particular previous turn. A beamlet will be specified by the number of the turn during which it was injected. By a turn-to-turn force we mean the electric force exerted by one beamlet on another.

The turn-to-turn forces are included in Chapter IV. They have a substantial effect on the resulting distribution. The cross section still has a rough circular symmetry, but the beam has a low density halo. The program provides a means of calculating the betatron oscillation frequencies of any beamlet during any turn. Plots of horizontal and vertical tunes versus time for selected beamlets, as well as the average tunes for all beamlets present in the machine clearly show the depression of tune due to the increasing space charge forces as injection proceeds. The proposed KV scenario produces a more uniform beam density and smaller tune

shifts than the other injection scenario. When the gradient bump is added the effect of the half-integral resonance is clearly seen in the tune plots. In cases where the tunes would otherwise cross the resonance at $v = 5.5$ during injection, the gradient bump causes the beam to expand when the resonance is reached and the tune levels off at a value corresponding to the edge of the stop band. The optimum parameters correspond to arranging that horizontal and vertical tunes both just reach the edge of the stop band at the end of injection. This gives the maximum injected beam for a given beam cross section without an expanded halo.

There appear to be two regimes when beams exceeding the space charge limit are injected. If one or both tunes start at a value not too far from the resonance stop band, then the resonance dominates the process and the beam has a halo which expands to keep the tune at the edge of the stop band. If we start with tunes far enough from the resonance, which requires injecting a more intense beam in order to reach the stop band, then the fluctuating turn-to-turn forces dominate the process and cause the beam to expand because of the resulting diffusion in betatron amplitudes. The resulting beam density profiles do not depend very much on whether the resonance driving bump is present or not, although even in this case the effect of the bump can clearly be seen in the plots of tunes versus time.

II. THEORY

In Section 1 we will derive the KV distribution for the smooth case when the betatron motion is a simple harmonic oscillator and the parameters are arranged to produce a circular beam cross section. Section 2 treats the full alternating gradient case and allows the beam cross section to be elliptical. Section 3 presents an injection scenario in which the x and y amplitudes during injection are programmed to paint the energy shell uniformly and so produce a KV distribution. Section 4 discusses an alternative way of producing a KV distribution using a small xy coupling.

1. A Simple KV Distribution.

We start from the simple Hamiltonian

$$H = \frac{1}{2}p_x^2 + \frac{1}{2}k_x x^2 + \frac{1}{2}p_y^2 + \frac{1}{2}k_y y^2 \quad , \tag{1.1}$$

where the independent variable is the azimuthal distance s. The moments are

$$p_x = \frac{dx}{ds} \quad , \quad p_y = \frac{dy}{ds} \quad . \tag{1.2}$$

We are assuming that the focussing forces are linear. The space charge forces for the KV distribution will also be linear, and are included in the constants k_x, k_y. The solution of the equations of motion is a simple harmonic oscillation in both dimensions of frequencies

$$v_x = Rk_x^{1/2} \quad , \quad v_y = Rk_y^{1/2} \quad , \tag{1.3}$$

in oscillations per revolution, where $2\pi R$ is the circumference.

Introduce angle-action variables:

$$x = (2RJ_x / v_x)^{1/2} \sin \gamma_x \quad , \quad p_x = \left(2v_x J_x / R\right)^{1/2} \cos \gamma_x \quad ,$$

$$y = (2RJ_y / v_y)^{1/2} \sin \gamma_y \quad , \quad p_y = \left(2v_y J_y / R\right)^{1/2} \cos \gamma_y \quad . \tag{1.4}$$

The Hamiltonian becomes

$$H = \frac{v_x}{R} J_x + \frac{v_y}{R} J_y \quad . \tag{1.5}$$

The action variables

$$J_x = \frac{Rp_x^2}{2v_x} + \frac{v_x x^2}{2R} \quad , \quad J_y = \frac{Rp_y^2}{2v_y} + \frac{v_y y^2}{2R} \tag{1.6}$$

are constants of the motion and are each equal to the area of the corresponding phase ellipse divided by 2π. The angle variables are

$$\gamma_x = v_x s / R + \vartheta_x \quad , \quad \gamma_y = v_y s / R + \vartheta_y \quad , \tag{1.7}$$

where ϑ_x, ϑ_y are arbitrary constants. If we substitute from Eqs.(1.7) into Eqs.(1.4), we get the general solution of the equations of motion.

Now write the distribution function for the beam in the form

$$D(J_x, J_y, \gamma_x, \gamma_y) = A\delta(2J_x \cos^2 \zeta + 2J_y \sin^2 \zeta - J_0) \quad . \tag{1.8}$$

This is a slight generalization of the standard microcanonical distribution, in that it allows J_x and J_y to appear with arbitrary factors in the total action J_0. It becomes a standard microcanonical distribution if we set $\zeta = \pi/4$. The advantage of introducing the parameter ζ is that it allows us to adjust the shape of the beam in x,y space; for example, we can change an ellipse into a circle, even when $k_x \neq k_y$.

The particle density in physical space is

4

$$\rho(x,y) = \int dp_x \int dp_y D(x,p_x,y,p_y)$$

$$= A \int dp_x \int \delta(2J_x \cos^2 \zeta + w - J_0) \frac{dw}{2\sin^2 \zeta \frac{\partial J_y}{\partial p_y}}$$

$$= \frac{A v_y^{1/2}}{2R^{1/2} \sin \zeta} \int_{-p_{x1}}^{p_{x1}} \frac{dp_x}{\left[J_0 - \left(\frac{Rp_x^2}{v_x} + \frac{v_x x^2}{R} \right) \cos^2 \zeta - \frac{v_y y^2}{R} \sin^2 \zeta \right]^{\frac{1}{2}}}$$

$$= \frac{(v_x v_y)^{1/2} A}{2R \sin \zeta \cos \zeta} \int_{-\pi/2}^{\pi/2} \frac{\cos \vartheta \, d\vartheta}{\left[1 - \sin^2 \vartheta \right]^{\frac{1}{2}}}$$

$$= \frac{\pi (v_x v_y)^{1/2} A}{R \sin 2\zeta} \quad , \qquad (1.9)$$

where we have put

$$w = 2J_y \sin^2 \zeta \quad ,$$

$$p_{x1} = \frac{v_x^{1/2}}{R^{1/2} \cos \zeta} \left[J_0 - \frac{v_x x^2 \cos^2 \zeta}{R} - \frac{v_y y^2 \sin^2 \zeta}{R} \right]^{\frac{1}{2}} \quad , \qquad (1.10)$$

$$p_x = p_{x1} \sin \vartheta \quad .$$

The density is constant (within the beam), which implies that the space charge force is linear, as we will see below. In evaluating the second line of Eq.(1.9), we have assumed that there are values of p_x, p_y for which the argument of the δ-function in Eq.(1.8) vanishes. This will be true provided the point x,y lies within the ellipse

$$\frac{v_x x^2 \cos^2 \zeta}{R} + \frac{v_y y^2 \sin^2 \zeta}{R} = J_o \quad . \qquad (1.11)$$

Outside this ellipse, the particle density is zero. The area of this ellipse is

$$A_e = \frac{2\pi R J_0}{\left[v_x v_y \right]^{1/2} \sin 2\zeta} \quad . \qquad (1.12)$$

Since the density (1.9) inside the ellipse is uniform, it is just the number N of particles per unit length divided by the area of the ellipse:

$$\rho(x,y) = \rho_0 = \frac{N[v_x v_y]^{1/2} \sin 2\zeta}{2\pi R J_0} \quad . \tag{1.13}$$

The electric field due to this particle density can be written

$$\mathbf{E} = -\nabla \phi \quad , \tag{1.14}$$

where the electric potential satisfies, inside the ellipse (1.11), the equation

$$\nabla^2 \phi = \frac{\partial^2 \phi}{\partial x^2} + \frac{\partial^2 \phi}{\partial y^2} = -\frac{e\rho_0}{\varepsilon_0} \quad , \tag{1.15}$$

and variations in the azimuthal direction are neglected. A solution of Eq.(1.15) is

$$\phi(x,y) = \phi_0 - \frac{1}{2}\kappa_x^2 x^2 - \frac{1}{2}\kappa_y^2 y^2 \quad , \tag{1.16}$$

where the constants κ_x and κ_y must satisfy

$$\kappa_x^2 + \kappa_y^2 = \frac{e\rho_0}{\varepsilon_0} \quad . \tag{1.17}$$

This condition can be satisfied by setting

$$\kappa_x = \kappa \cos\xi \quad , \quad \kappa_y = \kappa \sin\xi \quad , \tag{1.18}$$

where ξ is arbitrary and

$$\kappa^2 = \frac{e\rho_0}{\varepsilon_0} = \frac{Ne[v_x v_y]^{1/2} \sin 2\zeta}{2\pi\varepsilon_0 R J_0} \quad . \tag{1.19}$$

The general solution of Eq.(1.15) is obtained by adding to the solution (1.16) the general solution of the homogeneous equation

$$\frac{\partial^2 \phi}{\partial x^2} + \frac{\partial^2 \phi}{\partial y^2} = 0 \tag{1.20}$$

which is well-behaved at the origin. This must then be matched to a solution of Eq.(1.20) between the beam and the vacuum chamber. Since we are only looking for some self-consistent solution of the problem, we simplify the problem by taking a round beam:

$$\tan^2 \zeta = \frac{v_x}{v_y} \quad , \tag{1.21}$$

which makes Eq.(1.11) the equation for a circle:

$$x^2 + y^2 = a^2 = \frac{v_x + v_y}{v_x v_y} R J_0 \quad , \tag{1.22}$$

where a is the radius of the beam. Note that we have made the beam round without assuming that $v_x = v_y$. If they are equal then $\zeta = \pi/4$. In any case, we set $\xi = \pi/4$, so that the potential has circular symmetry. Inside the beam, the potential (1.16) is then

$$\phi(x,y) = \phi(r) = \phi_0 - \frac{1}{4}\kappa^2(x^2 + y^2) = \phi_0 - \frac{1}{4}\kappa^2 r^2 \quad . \tag{1.23}$$

Outside, the potential is

$$\phi(r) = C \ln \frac{r}{b} \quad , \tag{1.24}$$

where the additive constant is chosen to make the potential vanish at the vacuum chamber radius b. The potential and its radial derivative have to be continuous across the boundary. The potential is then

$$\phi(x,y) = \begin{cases} \dfrac{ea^2 \rho_0}{4\varepsilon_0}\left(1 + 2\ln\dfrac{b}{a}\right) - \dfrac{e\rho_0}{4\varepsilon_0}\left(x^2 + y^2\right) & \text{inside the beam} \quad , \\[4mm] -\dfrac{ea^2 \rho_0}{2\varepsilon_0}\ln\dfrac{r}{b} & \text{outside} \quad , \end{cases} \tag{1.25}$$

where

$$\rho_0 = \frac{N v_x v_y}{\pi R J_0 (v_x + v_y)} \quad . \tag{1.26}$$

The space charge forces in the non-relativistic limit (i.e., neglecting magnetic self-forces) are

$$F_x = -e\frac{\partial \phi}{\partial x} = \frac{e^2 \rho_0}{2\varepsilon_0} x \quad ,$$

$$F_y = -e\frac{\partial \phi}{\partial y} = \frac{e^2 \rho_0}{2\varepsilon_0} y \quad . \tag{1.27}$$

The constants k_x, k_y in Eq.(1.1) can now be written in terms of the external focussing force constants k_{ex}, k_{ey}:

$$k_x = k_{ex} - \frac{e^2 \rho_o}{2\varepsilon_0 \beta^2 \gamma^2 mc^2} \quad ,$$

$$k_y = k_{ey} - \frac{e^2 \rho_o}{2\varepsilon_0 \beta^2 \gamma^2 mc^2} \quad ,$$

(1.28)

where β and γ are the relativistic parameters, whose variation with s are neglected, m is the mass, and an extra factor γ is added to the denominators to include the effects of the magnetic forces.

We now have a complete, self-consistent solution of the equations of motion for a round beam, including the effects of space charge forces.

2. The KV Solution for an AG Ring.

We will derive the general Kapchinskij-Vladimirskij solution for an elliptical beam in an alternating gradient ring following the same steps as in the treatment of the simpler problem above. Our treatment is a generalization of the KV paper (1), since they eventually assume a round beam. We start with the Hamiltonian (1.1), but we allow the force coefficients to depend (periodically) on s:

$$H(x, p_x, y, p_y) = \frac{1}{2} p_x^2 + \frac{1}{2} p_y^2 + \frac{1}{2} k_x(s) x^2 + \frac{1}{2} k_y(s) y^2 \quad .$$

(2.1)

We will assume that the wavelengths for the variations of the functions $k_x(s)$, $k_y(s)$ are much longer than the cross sectional dimensions of the beam, so that the fields can be calculated treating the beam as a uniform elliptical cylinder at each azimuth s. The action variables are the Courant-Snyder invariants:

$$J_x = \frac{(\beta_x(s) p_x + \alpha_x(s) x)^2 + x^2}{\beta_x(s)} \quad ,$$

$$J_y = \frac{(\beta_y(s) p_y + \alpha_y(s) y)^2 + y^2}{\beta_y(s)} \quad ,$$

(2.2)

where the parameters $\alpha(s)$ and $\beta(s)$ are periodic functions of s.

We again write the generalized microcanonical distribution in the form (1.8). The calculation of the spatial density proceeds just as in the preceding section, and we get

8

$$\rho(x,y) = \int dp_x \int dp_y \, D(x, p_x, y, p_y)$$

$$= \frac{\pi A}{\left[\beta_x(s)\beta_y(s)\right]^{1/2}\sin 2\zeta} \quad , \tag{2.3}$$

within the ellipse

$$\frac{x^2 \cos^2 \zeta}{\beta_x(s)} + \frac{y^2 \sin^2 \zeta}{\beta_y(s)} = J_0 \quad , \tag{2.4}$$

and zero outside. The density is again uniform within the ellipse, but varies periodically in s, as does the area of the ellipse which is

$$A_e = \frac{2\pi J_0 \left[\beta_x(s)\beta_y(s)\right]^{\frac{1}{2}}}{\sin 2\zeta} \quad . \tag{2.5}$$

We will neglect any variation in the azimuthal velocity so that the linear density N (particles per unit length along s) is a constant of the motion. For a bunched beam, N may vary along the bunch, but remains constant at the location of any given particle at least for many revolutions, so its variation may be neglected in studying the betatron oscillations. The spatial density is then

$$\rho(x,y,s) = \rho_0(s) = \frac{N \sin 2\zeta}{2\pi J_0 \left[\beta_x(s)\beta_y(s)\right]^{\frac{1}{2}}} \quad . \tag{2.6}$$

We have to solve Eq.(1.15) which will be written in the form

$$\frac{\partial^2 \phi}{\partial x^2} + \frac{\partial^2 \phi}{\partial y^2} = \begin{cases} -\kappa^2(s) & \text{inside the beam} \quad , \\ 0 & \text{outside} \quad , \end{cases} \tag{2.7}$$

where $\kappa^2(s)$ is given by Eq.(1.17), with $\rho_0(s)$ given by Eq.(2.6), and the beam boundary is given by Eq.(2.4). We are assuming that the dependence on s is slow, so we neglect derivatives with respect to s.

In order to solve Eq.(2.7), one could write a solution in the form (1.16) or (1.23) inside the beam and try to fit the boundary condition at the wall and at the beam boundary by adding suitable solutions of the homogeneous equation inside and outside. Instead, since the beam boundary is an ellipse, we will use confocal elliptic coordinates (3, p.1195):

$$x = h \cosh \mu \cos \lambda \quad , $$
$$y = h \sinh \mu \sin \lambda \quad , \tag{2.8}$$

which gives ellipses of constant μ and hyperbolas of constant λ with foci at $x = \pm h(s)$, $y = 0$. The coordinate μ runs from 0 to ∞. The coordinate λ is an angle from 0 to 2π and is roughly equal to the polar angle θ. The (positive, negative) x-axis is given (outside the foci) by $\lambda = 0, \pi$; the y-axis is given by $\lambda = \pm\pi/2$. We choose as coordinate foci the foci of the ellipse (2.4):

$$h(s) = \left[\frac{\beta_x(s)J_0}{\cos^2\zeta} - \frac{\beta_y(s)J_0}{\sin^2\zeta}\right]^{\frac{1}{2}} , \qquad (2.9)$$

so that the ellipse (2.4) is an ellipse of constant $\mu = \mu_b$:

$$\frac{x^2}{h^2\cosh^2\mu_b} + \frac{y^2}{h^2\sinh^2\mu_b} = \frac{x^2\cos^2\zeta}{\beta_x J_0} + \frac{y^2\sin^2\zeta}{\beta_y J_0} = 1 , \qquad (2.10)$$

from which Eq.(2.9) follows. The elliptic coordinate of the beam ellipse is given by

$$\tanh\mu_b(s) = \left[\frac{\beta_y(s)}{\beta_x(s)}\right]^{\frac{1}{2}}\cot\zeta . \qquad (2.11)$$

We will usually omit explicit dependences on s, except when introducing a new quantity. Note that the ellipse of constant μ approaches a circle as μ becomes large (so that $\sinh\mu \doteq \cosh\mu$), and that the eccentricity approaches 1 for small μ. For $\mu = 0$ the ellipse shrinks to the line segment connecting the foci. The major axis of the beam ellipse is taken to be horizontal.

We will assume that the conducting vacuum chamber wall is also elliptical and confocal with the beam. The potential vanishes at the wall. In elliptic coordinates Eq.(2.7) becomes (3, p.504)

$$\frac{1}{h^2(\cosh^2\mu - \cos^2\lambda)}\left(\frac{\partial^2\phi}{\partial\mu^2} + \frac{\partial^2\phi}{\partial\lambda^2}\right) = \begin{cases} -\kappa^2 & \text{inside the beam} , \\ 0 & \text{outside} . \end{cases} \qquad (2.12)$$

This equation is to be solved keeping ϕ and its normal derivative continuous across the beam boundary, and with $\phi = 0$ at the wall which we take to be the ellipse $\mu = \mu_w$. A particular solution inside can be found either by solving Eq.(2.12) by separation of variables or by taking the solution (1.23) and substituting from Eq.(2.8). The result is

$$\phi = -\frac{\kappa^2 h^2}{4}(\cosh 2\mu + \cos 2\lambda) . \qquad (2.13)$$

To this we add a solution of the homogeneous equation inside, and another outside. A set of solutions of the homogeneous equation periodic in λ is

$$\phi = 1, \quad \phi = \mu,$$
$$\phi = \cosh m\mu \cos m\lambda,$$
$$\phi = \sinh m\mu \sin m\lambda,$$
$$\phi = \sinh m\mu \cos m\lambda,$$
$$\phi = \cosh m\mu \sin m\lambda,$$

(2.14)

where m is any positive integer. The second and the last two solutions are not well behaved at the origin, due in part to the peculiar behavior of the coordinate system near $\mu = 0$. The rest are polynomials of order m in x and y. It is clear from Eq.(2.13) that we need the solutions for $m = 0$ (the first two) and $m = 2$. We therefore write

$$\phi(\mu, \lambda) =$$

$$\begin{cases} \dfrac{\kappa^2 h^2}{4}\left[\cosh 2\mu + \cos 2\lambda - A + B\cosh 2\mu \cos 2\lambda\right] & \text{inside,} \\[2em] \dfrac{\kappa^2 h^2}{4}\left[C(\mu_w - \mu_b) - D(\cosh 2\mu \sinh 2\mu_w - \sinh 2\mu \cosh 2\mu_w)\cos 2\lambda\right] & \text{outside,} \end{cases}$$

(2.15)

where the coefficients are already adjusted to satisfy the boundary condition at the wall. We have to require that ϕ and $\partial\phi/\partial\mu$ be continuous at the beam ellipse; the result is

$$A = 2(\mu_w - \mu_b)\sinh 2\mu_b + \cosh 2\mu_b,$$
$$B = \frac{\cosh 2\mu_b \cosh 2\mu_w - \sinh 2\mu_b \sinh 2\mu_w}{\cosh 2\mu_w},$$
$$C = 2\sinh 2\mu_b,$$
$$D = \frac{\sinh 2\mu_b}{\cosh 2\mu_w}.$$

(2.16)

For comparison with the development in the previous section we would need the circular limit of the above equations where $h\to 0$ and $\mu \gg 1$ almost everywhere. In that limit $\cosh \mu$ and $\sinh \mu$ approach $(e^\mu)/2$, the ellipses become circles, and λ becomes the polar angle θ. In that limit, $\mu\to\ln 2r/h$.

The solution (2.15) inside the beam can be written

$$\phi = -\frac{\kappa^2 h^2}{4}(A + B) + \frac{1}{2}\kappa^2(x^2 + y^2) + \frac{B}{2}\kappa^2(x^2 - y^2),$$

(2.17)

11

from which the electric space charge forces follow:

$$F_x = -e\kappa^2(1+B)x \quad ,$$
$$F_y = -e\kappa^2(1-B)y \quad .$$

(2.18)

The coefficients in Eq.(2.1) can now be written in terms of the external focussing coefficients and the space charge forces:

$$k_x(s) = k_{ex}(s) - \frac{e\kappa^2(s)(1+B(s))}{\beta^2\gamma^2 mc^2} \quad ,$$

$$k_y(s) = k_{ey}(s) - \frac{e\kappa^2(s)(1-B(s))}{\beta^2\gamma^2 mc^2} \quad .$$

(2.19)

We now have a complete, self-consistent solution of the general KV problem. If the vacuum chamber wall is not an ellipse or is not confocal with the beam boundary then matching boundary conditions becomes more difficult. It may be necessary to add terms with $m > 2$ to the solution, in which case terms in x and y of order higher than two will appear in the solution (2.17). There will then be nonlinear terms in the forces (2.18) and our solution is no longer self-consistent. However for a reasonable wall shape one would expect such terms to be small, especially inside the beam. In any case, if beam and vacuum chamber are circular, the distribution (2.4) will result in linear space charge forces. For a circular beam in a concentric circular vacuum chamber, the KV distribution (2.4) always leads to linear focussing forces.

3. The Painting Scenario.

The KV distribution is essentially a microcanonical distribution with the beam distributed uniformly over a three-dimensional energy shell corresponding to a fixed total energy in the four-dimensional phase space of the x and y betatron oscillations. We need to construct a scenario which allows us to paint the energy shell uniformly. To simplify the treatment, our discussion will be based on the treatment in Section 1 which starts from the smoothed Hamiltonian (1.1).

If we inject at a fixed point in the phase space, the betatron oscillations will spread the beam over the γ_x, γ_y phase plane. In order to spread it over the three-dimensional surface defined by Eq.(1.8), we need to vary the action variables in an appropriate way. To this end introduce the variables

$$J_0 = 2\cos^2\zeta\, J_x + 2\sin^2\zeta\, J_y \quad ,$$

$$J_m = 2\cos^2\zeta\, J_x - 2\sin^2\zeta\, J_y \quad .$$

(3.1)

The Jacobian of this transformation is constant. Therefore if area is conserved in the $J_x J_y$ phase plane then it is also conserved in the $J_0 J_m$ phase plane.

The total action J_0 is to be held constant and J_m is to be varied slowly. If the variation of J_m is slow compared with the betatron frequencies, then near each value

of J_m the betatron motion will distribute the injected beam uniformly over the γ_x, γ_y phase plane, provided there is no rational relation with small denominator between ν_x and ν_y. The J_0 shell must be painted uniformly, so we require that dJ_m/dt be constant:

$$J_m = -J_0\left(1 - \frac{2t}{T}\right) \quad , \tag{3.2}$$

where T is the total injection time. Note that we want to paint both positive and negative values of J_m. Equation (3.2) is adjusted for the case in which $J_m = -J_0$ initially, i.e., the y amplitude is maximum and the x amplitude is zero. The injected x,y actions are given by

$$J_x = \frac{1}{2\cos^2\zeta} J_0 \frac{t}{T} \quad ,$$

$$J_y = \frac{1}{2\sin^2\zeta} J_0\left(1 - \frac{t}{T}\right) \quad . \tag{3.3}$$

The painting scenario can be achieved in the IPNS upgrade by using H(-) injection with a stripping foil, an internal horizontal orbit bump, and an external vertical deflection of the injected beam.

4. The Coupling Scenario.

Yanglai Cho (4) has pointed out that coupling the x and y betatron motions may allow us to achieve a KV distribution. He proposes to make the x and y betatron tunes equal and provide a small coupling between them. Then inject with zero y amplitude and a large fixed x amplitude. The coupling causes the y oscillation energy to increase at the expense of the x energy. This has two effects. First, it causes the previously injected beamlet to move away from the inflector and remain away for one beat period, thus facilitating multi-turn injection. Second, it results in a distribution in which all particles have the same total oscillation energy.

Unfortunately this procedure does not result in a microcanonical distribution, since it does not fill the energy shell uniformly. It fills only a two-dimensional torus scanned by the phases of the two coupled normal modes. Filling the three-dimensional energy shell requires also sweeping a suitably chosen variable analogous to J_m in Eq.(3.1). We have carried out the analysis [(5), Section 4] and have carried out corresponding simulations for this scenario. The results are similar to those presented later for the painting scenario. Since the coupling scenario seems to have no advantages over the painting scenario, we omit further discussion in this paper.

13

III. DOES IT WORK? — SIMULATION

5. Injecting with Painting Scenario.

We have written a program to simulate the scenario (3.3) as applied to the IPNS Upgrade (2). The injection time T corresponds to 500 injected turns. The maximum injected x-amplitude is 50 mm Figure (5.1) shows the x and y amplitudes of each beamlet as it is injected. The points lie on a circle beginning with zero x amplitude and maximum y amplitude at turn 1 and ending with zero y amplitude and maximum x amplitude at turn 500.

Figure (5.2) shows the resulting density in xy space at the end of injection. Each of the small circles represents one injected beamlet. The spatial density is fairly uniform within a circle. Figure (5.3) shows the final space charge shifted horizontal tunes of the 500 beamlets. The vertical tunes are similar. In these calculations, the space charge forces between beamlets are omitted, except at the end of the injection process when we turn on the interaction forces for one turn in order to calculate the space charge shifted tunes resulting from the density shown in Fig.(5.2).

6. Injecting with Non-KV Scenarios.

Figure (6.1) shows the injected amplitudes for a non-KV scenario. It differs from that shown in Fig.(5.1) in that the sum of the amplitudes is held constant instead of the sum of the actions (proportional to amplitudes squared). Although Figs.(5.1) and (6.1) are not much different, the resulting density distribution shown in Fig.(6.2), in contrast to that in Fig.(5.2), is neither circular nor uniform. Likewise the space-charge shifted tunes after injection, shown in Fig.(6.3) are not all equal as in Fig.(5.3).

IV. DOES IT REALLY WORK? — SIMULATION WITH SPACE CHARGE FORCES.

7. Simulation and Tune Measurement.

In order to include the effect of space charge forces, we calculate at each integration step the total force on each beamlet due to each of the other beamlets. In this way we include not just the Vlasov term, containing the smoothed out space charge force, but also the fluctuating beamlet-beamlet forces. In addition the equations of motion include for each beamlet terms like that on the right side of Eq.(7.2) below, to drive the resonance $v = 5.5$ for both x and y motions. The force between two beamlets is inversely proportional to the distance between them unless they overlap, in which case, the force drops linearly to zero as their centers approach one another.

In order to find the tune of a simulated beamlet, we find the average space charge force over one turn in the following way. We assume that we may
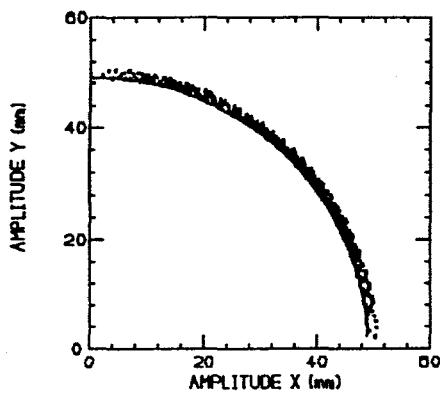
FIGURE 5.1 Painting scenario -
Injection amplitudes.
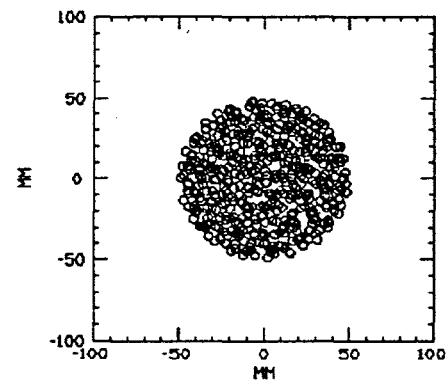
FIGURE 5.2 Painting scenario -
Final density.
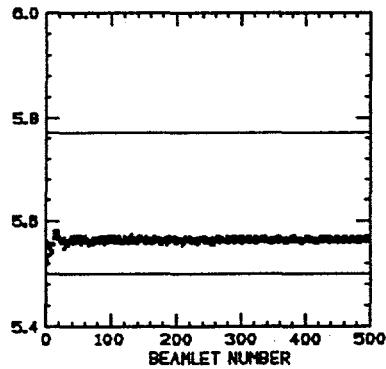
FIGURE 5.3 Painting scenario -
Final x tunes.
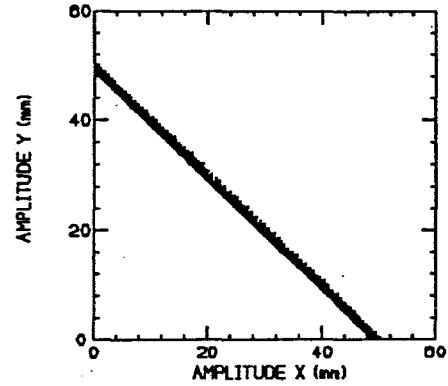
FIGURE 6.1 Non-KV scenario -
Injection amplitudes.
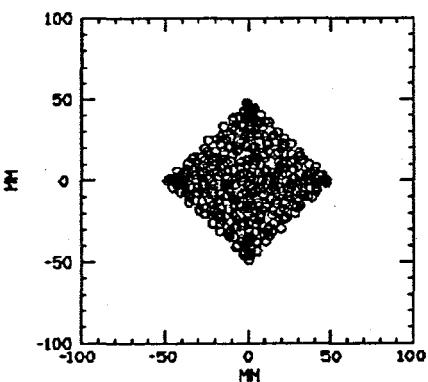
FIGURE 6.2 Non-KV scenario -
Final density.
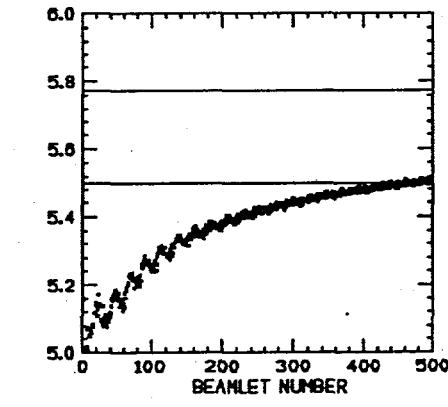

FIGURE 6.3 Non-KV scenario -
Final x tunes.
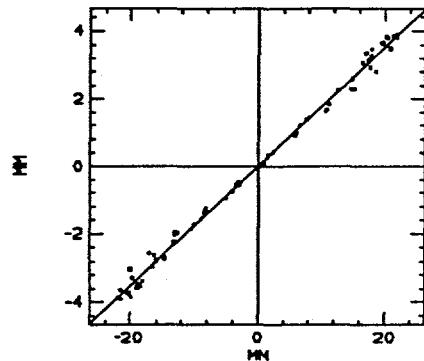
FIGURE 7.1 Force vs position for a
beamlet during one turn.
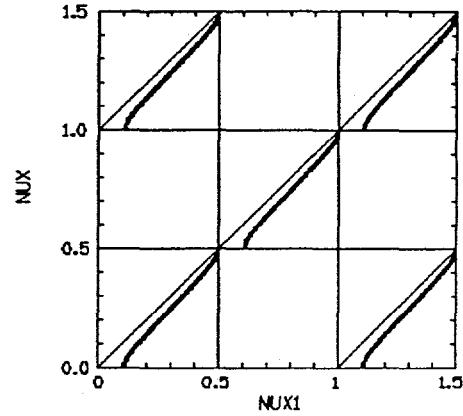
FIGURE 7.2 Tune vs. tune parameter.

approximate the average space charge force on any beamlet by a linear function of the displacement x (horizontal or vertical). The integration time step is Δs. At each integration step, we calculate the total momentum increment Δp of any given beamlet due to the forces from all other beamlets. Figure (7.1) shows a plot of $R\,\Delta p_x$ vs x for a typical beamlet at each integration step during one turn. The least squares linear fit to the data is also shown in the figure and is written in the form

$$\frac{\Delta p}{\Delta s} = Ax + B \ . \tag{7.1}$$

We then assume we may approximate the equation of motion by the linear equation

$$x'' + R^{-2}v_0^2 x - Ax = B + ax\delta(s - \pi R) \ , \tag{7.2}$$

where $R^{-2}v_0^2 x$ is the mean focussing from the lattice structure and the last term represents a quadrupole error term which is introduced to drive a possible half-integral resonance. The delta function is periodic with period $2\pi R$. The quadrupole bump is placed half way around the ring so that the reference point $s = 0$ is a symmetry point for the bumped lattice. Since the equilibrium orbit $x = x_e$ must satisfy Eq.(7.2), the deviation from the equilibrium orbit satisfies the homogeneous linear equation

$$(x - x_e)'' + R^{-2}(v_0^2 - S)(x - x_e) = a(x - x_e)\delta(s - \pi R) \ , \tag{7.3}$$

where

16

$$S = AR^2 \tag{7.4}$$

is the space charge defocussing coefficient. For algebraic convenience we will henceforth take x to be the deviation from the bumped equilibrium orbit and replace $x-x_e$ by x.

The phase vector is carried from s=0 to s=πR, (from the reference point to just before the bump), via a matrix **A**:

$$\begin{pmatrix} x \\ p \end{pmatrix}_{\pi R} = \mathbf{A} \begin{pmatrix} x \\ p \end{pmatrix}_0 \quad . \tag{7.5}$$

The matrix **A** is given by

$$\mathbf{A} = \begin{pmatrix} \cos\dfrac{\sigma_1}{2} & \sin\dfrac{\sigma_1}{2} \\ -\sin\dfrac{\sigma_1}{2} & \cos\dfrac{\sigma_1}{2} \end{pmatrix} \quad , \tag{7.6}$$

where

$$\sigma_1 = 2\pi \left(v_0{}^2 - S\right)^{1/2} \tag{7.7}$$

is the phase advance for the normal lattice plus space charge but without the gradient bump. We will call the quantity $(v_0{}^2 - S)^{1/2}$ the (horizontal or vertical) *tune parameter*. It is the space charge shifted tune in the absence of any resonance driving term. The matrix which carries the phase vector across the bump at $s=\pi R$ is

$$\mathbf{B} = \begin{pmatrix} 1 & 0 \\ -a & 1 \end{pmatrix} \quad . \tag{7.8}$$

The matrix which carries the phase vector once around the ring is then

$$\mathbf{M} = \mathbf{ABA} = \begin{pmatrix} \cos\sigma_1 - \dfrac{a}{2}\sin\sigma_1 & \sin\sigma_1 - \dfrac{a}{2}(1-\cos\sigma_1) \\ -\sin\sigma_1 - \dfrac{a}{2}(1+\cos\sigma_1) & \cos\sigma_1 - \dfrac{a}{2}\sin\sigma_1 \end{pmatrix} \quad . \tag{7.9}$$

The trace of **M** gives the phase advance σ around the ring:

$$\cos\sigma = \cos\sigma_1 - \frac{a\sin\sigma_1}{2} \quad . \tag{7.10}$$

If we consider σ as a function of σ_1 (or of the tune parameter) there will be unstable stop bands at integer and half integer resonances, i.e. at $\sigma=2n\pi$, where n is

17

an integer or half-integer. Let us assume that a is small and neglect all but the lowest order terms in a. If $a=0$, a solution of Eq.(7.10) is $\sigma=\sigma_1$. For small a Eq.(7.10) may be written in the form

$$\cos\sigma_1\left(1-\frac{(\sigma-\sigma_1)^2}{2}\right)-(\sigma-\sigma_1)\sin\sigma_1=\cos\sigma_1-\frac{a\sin\sigma_1}{2} \quad , \qquad (7.11)$$

where we have kept terms of order $(\sigma-\sigma_1)^2$ since near the stop bands $\sin\sigma_1$ is small of order a and all terms in Eq.(7.11) are second order. The solution of Eq.(7.11) is

$$\sigma=\sigma_1-\tan\sigma_1\left(1\pm\left[1+\frac{a}{\tan\sigma_1}\right]^{\frac{1}{2}}\right) \quad . \qquad (7.12)$$

Away from the resonance (i.e., $\tan\sigma_1 \gg a$) the solution (7.12) is, to lowest order in a,

$$\sigma=\sigma_1+\frac{a}{2} \quad . \qquad (7.13)$$

This solution is valid away from the integer and half-integer resonances. There is a second solution but it is not valid since it corresponds to $\sigma-\sigma_1 \gg a$. The edges of the stop bands occur where the solution of Eq.(7.10) is $\cos\sigma=\pm1$. One edge will be at $\sigma_1=2n\pi$. The other edge, to first order in a, occurs where the square root in Eq.(7.12) vanishes, at

$$\sigma_1 \doteq 2n\pi-a \quad . \qquad (7.14)$$

In the stop band the solution of the equation of motion has the form

$$x=e^{\pm\Gamma}e^{\pm2\pi i n s/R} \quad , \qquad (7.15)$$

with a growth rate approximately

$$\Gamma \doteq \left[-(\sigma_1-2n\pi)(\sigma_1-2n\pi+a)\right]^{1/2} \doteq a/2 \quad , \qquad (7.16)$$

where the last member is the growth rate at the center of the stop band. Since the growth rate has a vertical slope as a function of σ_1 at the edges of the stop band, it is roughly equal to $a/2$ throughout most of the stop band.

In Fig.(7.2) $\nu=\sigma/2\pi$ is plotted as a function of the tune parameter $\nu_1=\sigma_1/2\pi=(\nu_0^2-S)^{1/2}$. Note that according to Eq.(7.10) σ is a periodic function of σ_1. Figure (7.3) is a typical plot of the calculated shifted tune ν_y of a beamlet as a function of time. In this case a number of the calculated values lie in the stop band and are plotted at the top of the figure. In order to include values which lie in the

18
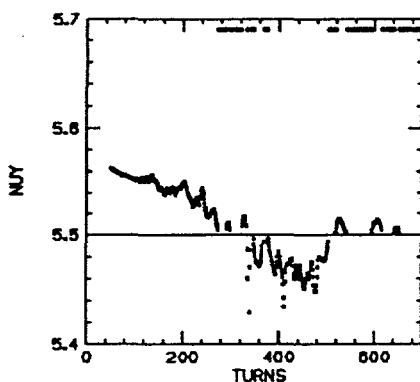
FIGURE 7.3 Tune vs. time for a typical beamlet.
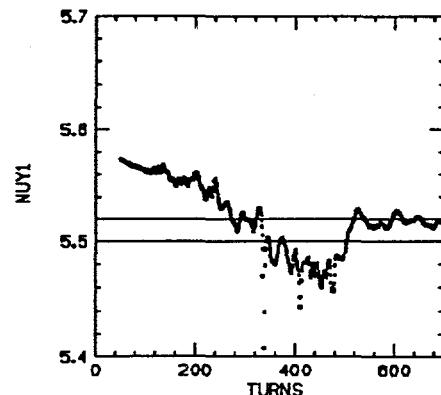
FIGURE 7.4 Tune parameter vs. time for the beamlet of Fig.(7.3).

stop band, we will generally plot the tune parameter $v_1 = (v_0{}^2\text{-}S)^{1/2}$ as in Fig.(7.4), which also shows the edges of the stop band. Outside the stop band the tune parameter is nearly equal to the actual tune. Inside the stop band the motion is unstable with a growth rate given by Eq.(7.16). Note that there are substantial fluctuations of the calculated tunes. These are due to the fluctuating character of the turn-to-turn space charge forces. In the tune calculation the actual space charge forces are replaced with mean linear approximations which are also subject to fluctuations from turn to turn.

8. Effect of Beamlet-Beamlet Forces.

The beam density for the KV scenario [Fig.(5.1)] with the space charge forces included is shown in Fig.(8.1). The beam is still roughly circular, but is not as
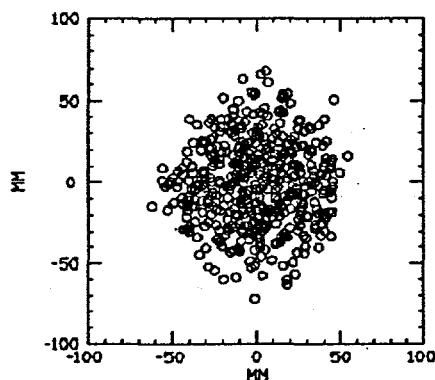
FIGURE 8.1 Final density for KV scenario with space charge.
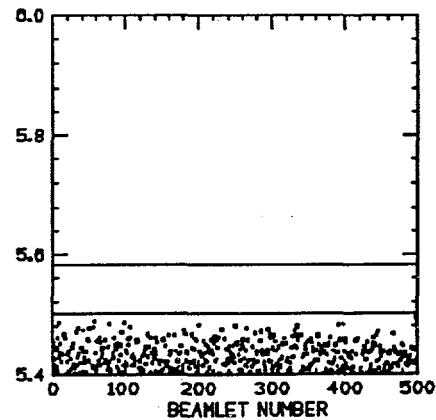
FIGURE 8.2 Final x tunes for KV scenario with space charge.

19
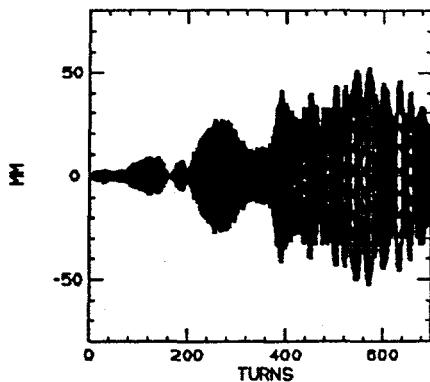
FIGURE 8.3 x coordinate during
KV injection with space charge.
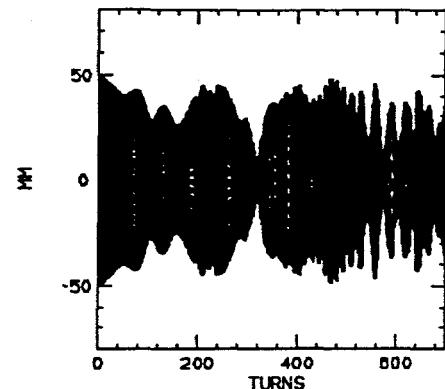
FIGURE 8.4 y coordinate during
KV injection with space charge.

uniform as in Fig.(5.2). As a result, the final tunes shown in Fig.(8.2) are not as constant as in Fig.(5.3). During injection, the beam does not yet have a KV distribution, so there are nonlinear space charge forces. There are also coupling forces between beamlets whose effects can be seen in Figs.(8.3) and (8.4) which show the x and y coordinates of the first injected beamlet as it passes the reference point during injection. Either the nonlinear space charge forces or diffusion due to beamlet-beamlet forces may be responsible for the non-uniformity of the beam in Fig.(8.1).

Figures (8.5) and (8.6) show the average x and y tunes, averaged over all injected beamlets, vs. turn number during the injection process. The two outer curves in these figures are the rms deviations from the average tunes. The increasing depression of the tunes due to the increasing space charge forces is evident. The tunes are depressed below the resonance at v = 5.5 because there is as yet no term in the simulation to drive the resonance.
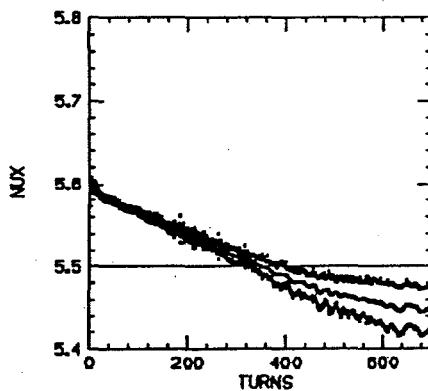
FIGURE 8.5 x tune during
KV injection with space charge.
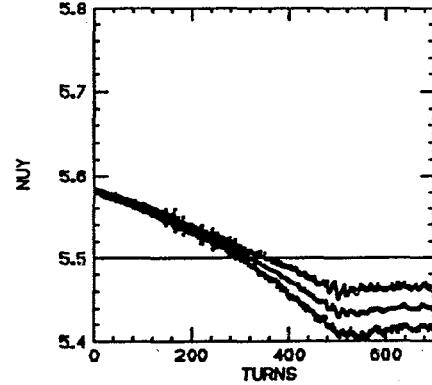
FIGURE 8.6 y tune during
KV injection with space charge.

20
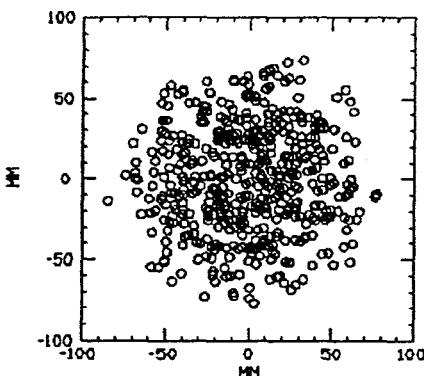
FIGURE 9.1 Final density for KV injection with resonance included.
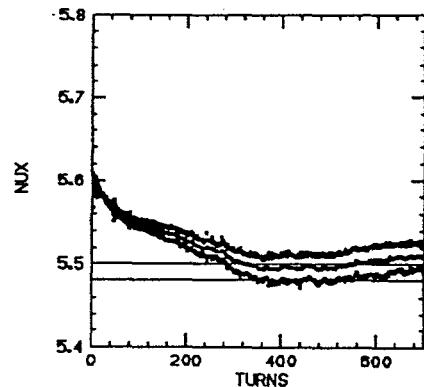
FIGURE 9.2 x tune parameters during KV injection with resonance included.

9. Effect of an Imperfection Resonance.

Using the same injection scenario with a gradient bump included to drive the resonance ν=5.5, the final density distribution is shown in Fig.(9.1) The x tunes during injection are shown in Fig.(9.2). The effect of the resonance on the tune history can be clearly seen. The resonance causes the beam density to expand to keep the tunes out of the stop band. The total injected current for this case is 27 A, with a bunching factor of 0.75. This is greater than required to depress the tune to the resonance and hence exceeds the conventionally defined space charge limit. We have also seen cases with large injected beam currents where the tune changes so rapidly that it can cross the resonance before the beam has time to expand.

10. The Space Charge Limited Case.

In a realistic case where we wish to inject the maximum possible beam without seriously increasing the beam size, we would choose an initial tune as far from the half-integral resonance as possible, and inject just enough beam to reduce the tunes to the edges of the stop bands. This corresponds to the conventional definition of the space charge limit. Figures (10.1), (10.2) and (10.3) show the final density and the tune history for this case, following the KV scenario (5.1). The total injected current is 54 A. The simulated tune shifts in Figs.(10.2) and (10.3) are equal to those calculated from the Laslett formula, as they should be if the simulation is done correctly.

Figures (10.4) and (10.5) show the same case for injection with the non-KV scenario. The final density is not much different, although the approach to resonance is more rapid in this case. For this case which starts far from the resonance and with a large injected beam, it would appear that the final density distribution is not dominated by the resonance, but instead is dominated by either the beamlet-beamlet collisions or the nonlinearities in the space charge forces or both. To illustrate this, we show in Fig.(10.6) the final density for the same case

21
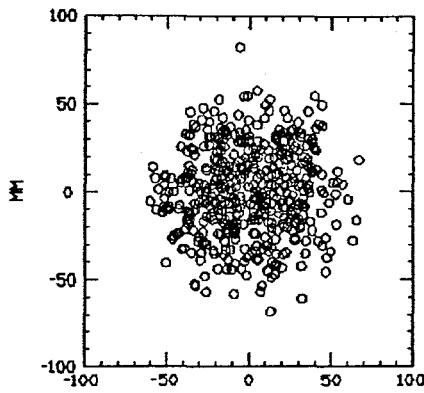
FIGURE 10.1 Final density , KV injection,
space charge limited case.
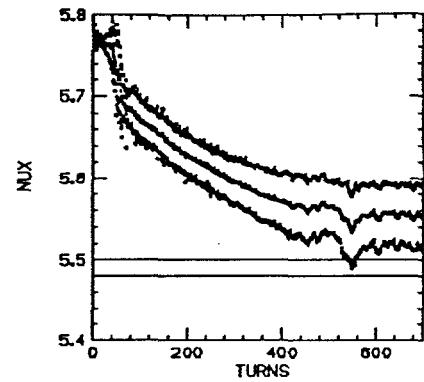
FIGURE 10.2 *x* tune parameter during
KV injection, space charge limited case.
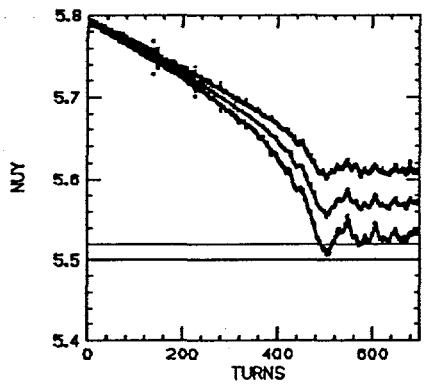
FIGURE 10.3 *y* tune parameter during
KV injection, space charge limited case.
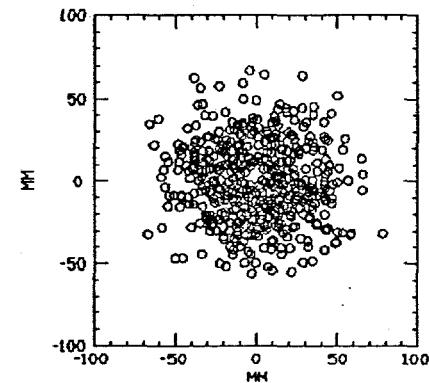
FIGURE 10.4 Final density, non-KV
injection, space charge limited case.
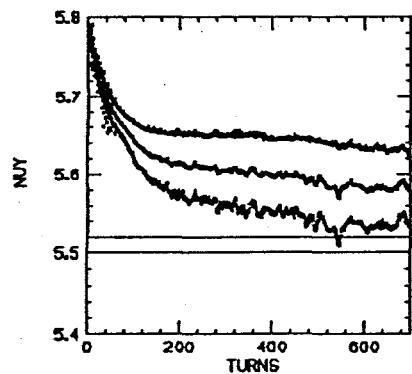
FIGURE 10.5 *x* tune parameter during
non-KV injection .
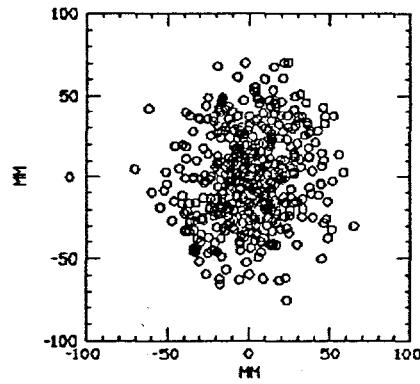
FIGURE 10.6 Final density, same case as
Fig.(10.4), without resonance.

but with the bump that drives the resonance turned off. There is little difference in the final density in Figs.(10.4) and (10.6).

V. CONCLUSIONS.

We have presented the theory of the KV distribution, including alternating gradient effects, and including the case of an elliptical beam. We have presented practical injection scenarios which lead to KV distributions if space charge forces are neglected during injection. The resulting distributions are uniform and circular (or elliptical), and result in uniform space charge shifted tunes for all particles.

When the effects of space charge and of beamlet-beamlet forces are included, injection with a KV scenario may have some advantage, but the resulting distribution is not exactly a KV distribution and the density is not exactly uniform. Two regimes may be distinguished. If the initial tunes are close to the resonance, the final density distribution is dominated by the amplitude growth of particles in the resonance stop band. This growth limits the space charge detuning so that the final tunes lie just above the stop band. If the initial tunes are far from resonance, and the injected beam intensity is large, the final density distribution is dominated by space charge effects — nonlinear forces and/or beamlet-beamlet collisions. This may mean that the effective space charge limit may sometimes occur at a beam intensity where the beam blow-up reaches the maximum acceptable value before the maximum acceptable tune shift is reached.

REFERENCES.

1. Kapchinskij,I. M. and Vladimirskij,V. V., "Limitations of Proton Beam Current in a Strong Focusing Linear Accelerator Associated with the Beam Space Charge," in *Proc. CERN Symposium on High Energy Accelerators, I* , 1959, pp. 274–288.
2. "IPNS Upgrade - A Feasibility Study," ANL-95/13, April 1995.
3. Morse, P.M. and Feshbach, H., *Methods of Theoretical Physics,* New York: McGraw-Hill, 1953.
4. Cho,Y., private communication.
5. Symon, K. R. "Kapshinskij-Vladimirskij Distribution," Argonne National Laboratory Neutron Source Accelerator Note NSA-95-5 (available on request).